Supporting Information

Nd Doping Bismuth Ferrite to Tune Electromagnetic Properties and Increase Microwave Absorption by Magnetic-dielectric Synergy

Yong Li,[a] Wen-qiang Cao,[b] Jie Yuan,*[b] Da-wei Wang[a] and Mao-sheng Cao*[a]

[a]School of Material Science and Engineering, Beijing Institute of Technology, Beijing, 10008, China

E-mail: caomaosheng@bit.edu.cn

[b]School of Science, Minzu University of China, Beijing 10008, China

E-mail: yuanjie4000@sina.com

Experimental section

Materials

Sol–gel method was employed to prepare BFO and BNFO nanoparticles. $Bi(NO_3)_3 \cdot 5H_2O$, $Fe(NO_3)_3 \cdot 9H_2O$ and $Nd(NO_3)_3 \cdot 6H_2O$ as raw materials in stoichiometric proportions were dissolved in 2-methoxyethanol. Citric acid in 1:1 molar ratio with respect to the metal nitrates was added to the solution, followed by polyethylene glycol as a dispersant. The mixture was stirred at 50 °C for 30 min to obtain the sol, and then it was dried at 80 °C to form the gel. The dried gel was calcined at 300 °C for 0.5 h. The calcined powders were sintered at 500 °C for 2 h.

Characterizations and measurements

The structure of the samples was collected using a X´Pert PRO system (Cu-K_α). Rietveld refinement of the XRD patterns was performed by using the FullProf Program. The morphologies were measured using S-4800 SEM system. The microstructure were determined by a JEM-2100 TEM system. Raman spectra were obtained using a HR800 Raman spectromater. XPS spectra were measured on a PHI Quantera system. The DC conductivity measurements were carried out using an Keithley 2401A-6517B multi-meter. Magnetic properties were measured by a Lakeshore 7407

vibrating sample magnetometer. The complex permittivity and permeability was measured on an Anritsu 37269D vector network analyzer by the waveguide method in X-band.

First-principles calculations

The calculations on density of states were performed using the CASTEP program code based on the first-principles plane-wave pseudo-potential method. The generalized gradient approximation (GGA) was adopted along with the exchange-correlation function realized by Perdow-Burke-Emzerhof (PBE). The plane wave cutoff energy of 500 eV and 2×2×2 *K*-point Monkhorst-Pack grid were applied to guarantee a well-converged structure under study. A $2a \times 2b \times$ c supercell was adopted for all the calculations.

Table S1. Microwave absorption performance of representative bismuth ferrite materials

Samples	f (GHz)	Min.RL (dB)	BW_{eff} (GHz)	BW_p (%)	d (mm)	Refs
$BiFeO_3$ nanoparticles	12.4–18	-26	4.8	85.7	3.5	23
$BiFeO_3$ ceramics	0–18	-17	0.8	4.4	5	24
$BiFeO_3$ ceramics	12.4–18	-23	3.5	62.5	1.2	25
$Bi_{0.85}Ho_{0.15}FeO_3$/paraffin wax composite	2–18	-11	0.5	3.1	3	26
$Bi_{0.8}La_{0.2}FeO_3$ nanoparticles	8.2–12.4	-30	1	17.8	6	27
$Bi_{0.8}Nd_{0.2}FeO_3$ nanoparticles	8.2–12.4	-42	3	71.4	2.3	This work

f, frequency range; Min.*RL*, minimum reflection loss; BW_{eff}, effective bandwidth ($RL \leq$ -10 dB); BW_p, the proportion of effective bandwidth in the frequency range investigated; *d*, thickness.

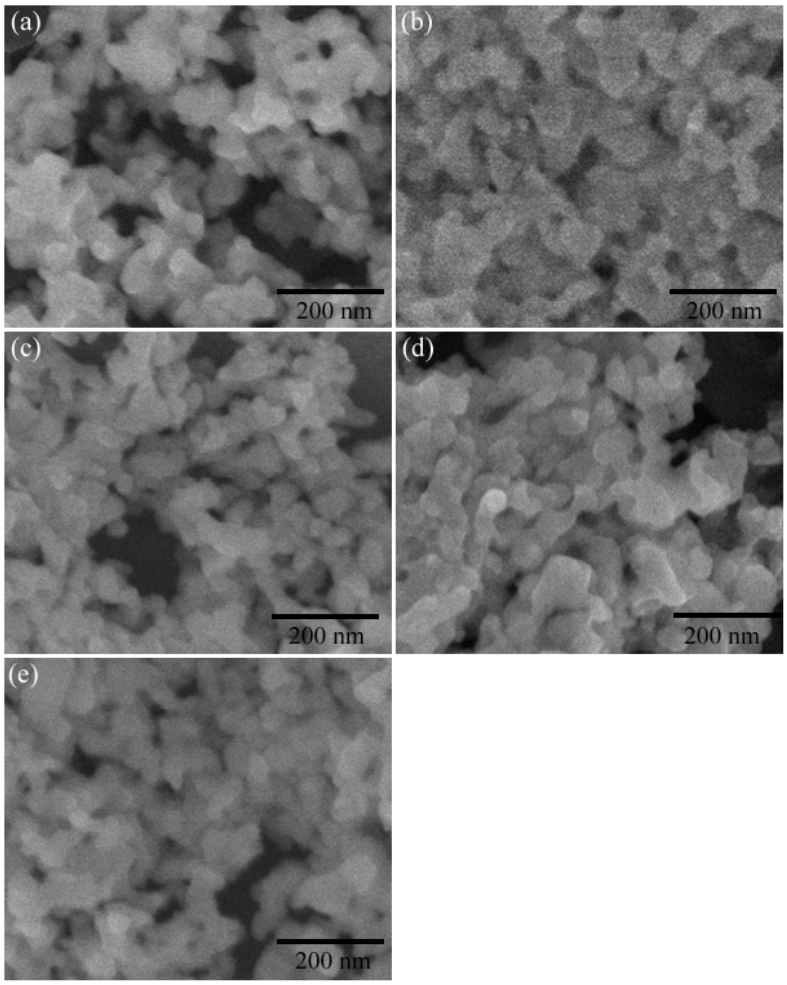

Fig. S1 SEM images of (a) BFO, (b) BNFO5, (c) BNFO10, (d) BNFO15 and (e) BNFO20 powders.

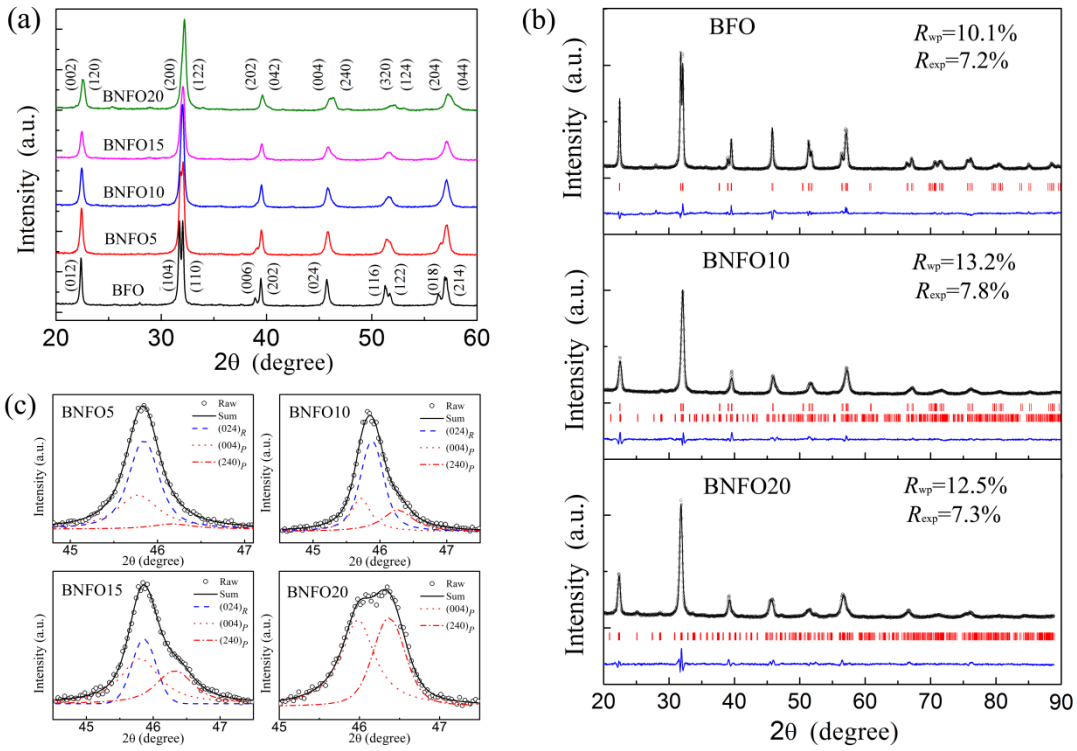

Fig. S2 (a)The XRD patterns of BFO and BNFO. (b) Rietveld refinement of BFO, BNFO10 and BNFO20: experimental (circle), calculated (black line). (c) The separated diffraction peaks in the range 2θ = 45-47°. The XRD patterns and Rietveld refinement of BFO and BNFO demonstrate that BFO is single phase perovskite with the *R*3*c* space group, while BNFO20 possesses the $PbZrO_3$-like structure as confirmed using the *Pbam* space group. In the intermediate compositions, the *R*3*c* phase and the *Pbam* phase coexist. The separated diffraction peaks in the range 2θ = 45-47° show that the intensity of $(0\ 0\ 4)_P$ and $(2\ 4\ 0)_P$ of the *Pbam* phase increases while the intensity of $(0\ 2\ 4)_R$ of the *R*3*c* phase decreases with the increase of Nd concentration, indicating the proportion of the *Pbam* phase increases gradually.

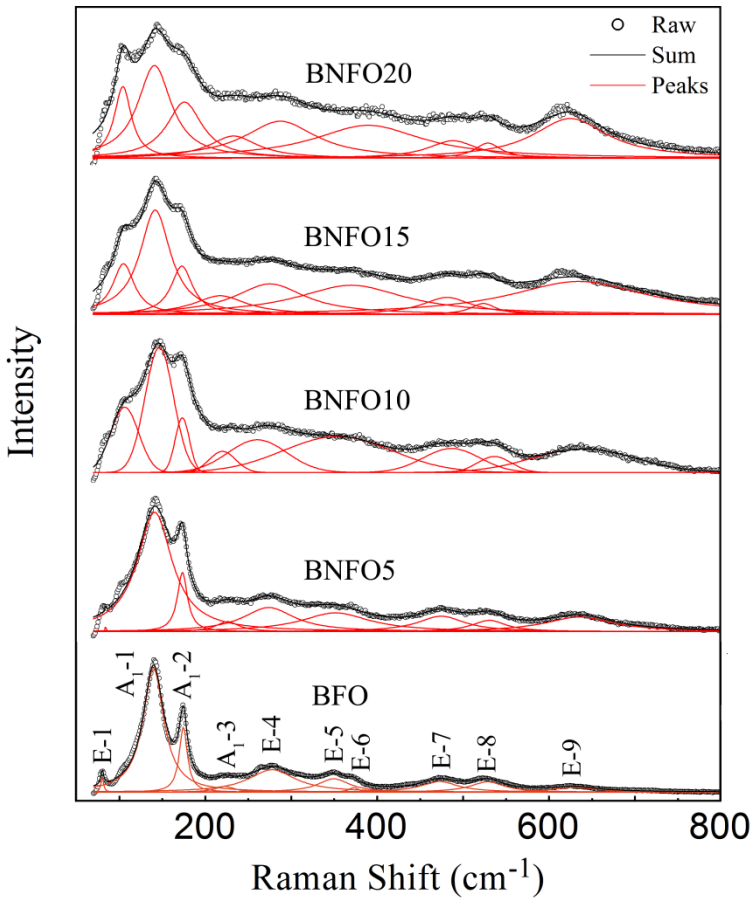

Fig. S3 Raman spectra of BFO and BNFO at room temperature. The *E*-1, A_1-1, A_1-2 and A_1-3 modes dominated by the Bi–O covalent bonds weaken with the increase of Nd concentration, indicating weakening of the hybridization of Bi 6*s* and O 2*p* orbits.

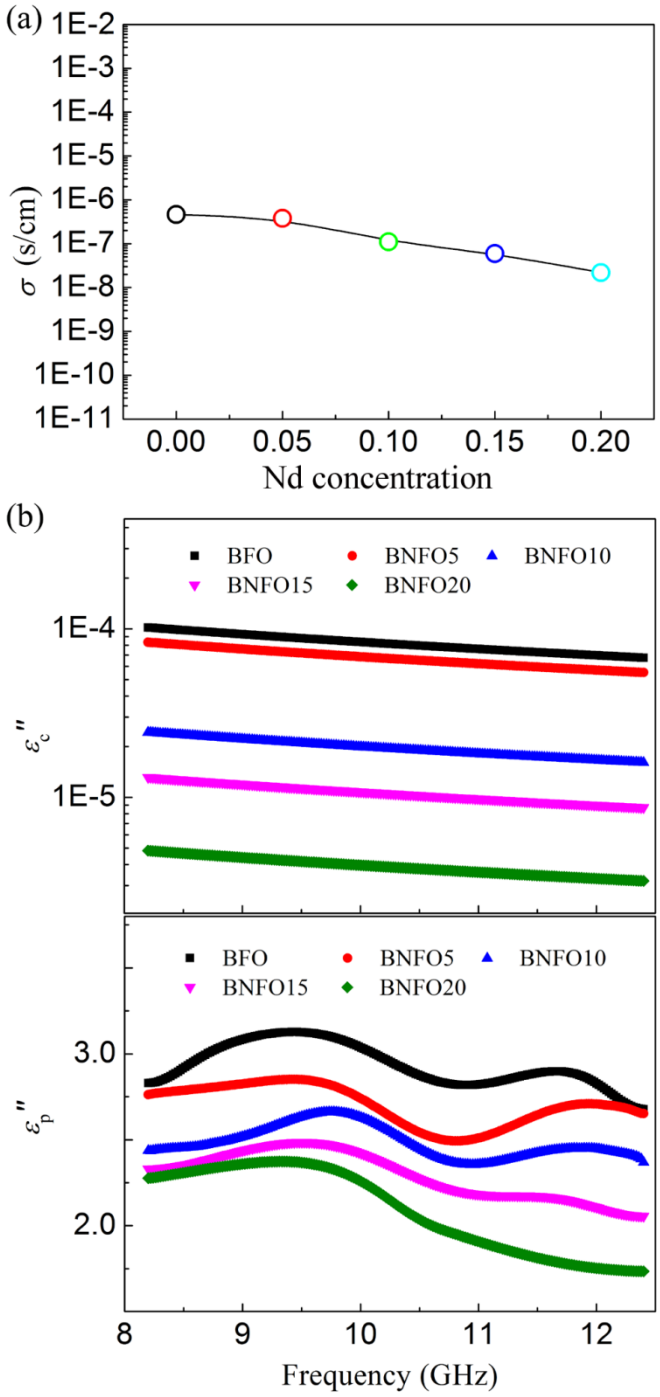

Fig. S4 (a) The DC conductivity versus Nd concentration at room temperature. (b) The conduction part (ε_c'') and polarization part (ε_p'') of imaginary permittivity for BFO and BNFO versus frequency. The ε_c'' is obtained based on Debye equation, i.e. $\varepsilon_c'' = \sigma/(\varepsilon_0\omega)$, where ε_0 is vacuum permittivity, ω is angular frequency and σ is conductivity of medium. Subtracting the ε_c'' from the imaginary permittivity, the ε_p'' is gained.

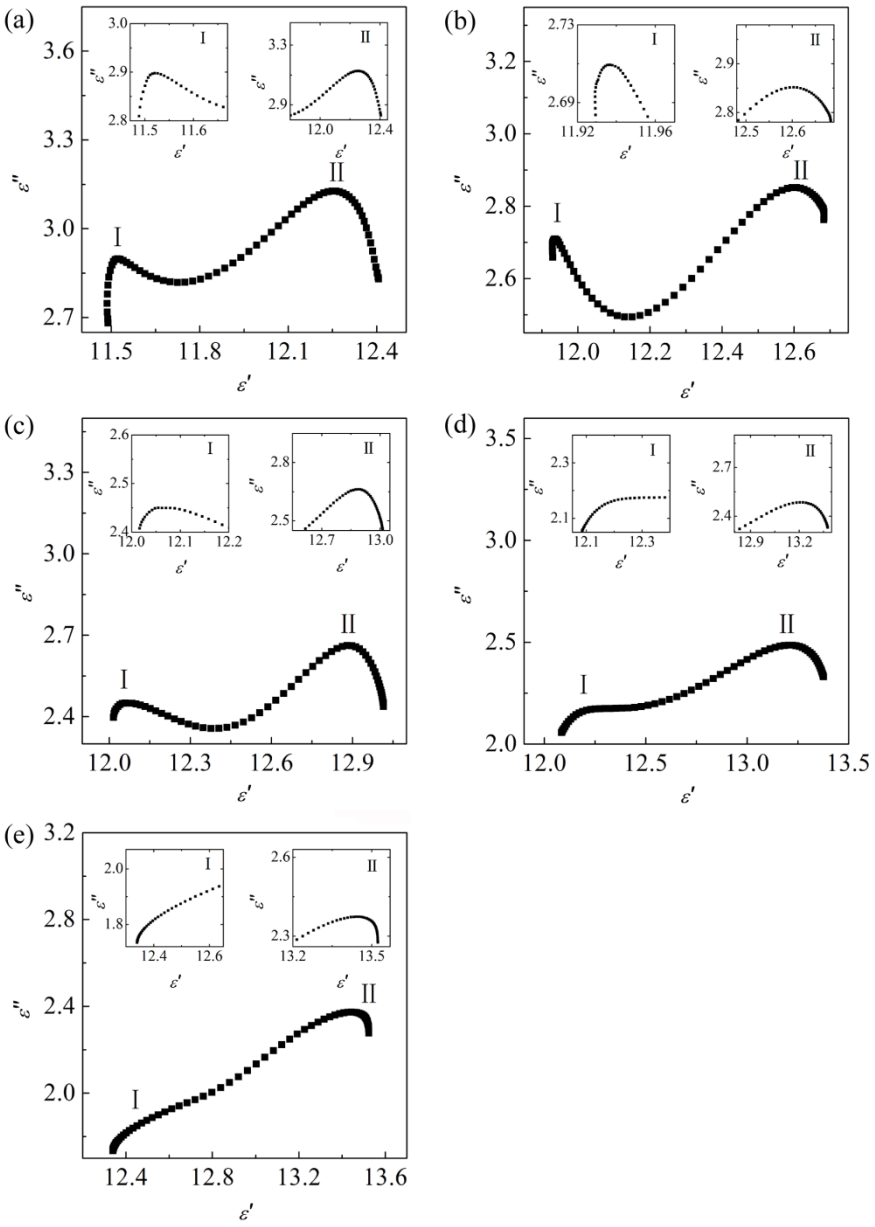

Fig. S5 The Cole-Cole plots of (a) BFO, (b) BNFO5, (c) BNFO10, (d) BNFO15 and (e) BNFO20.

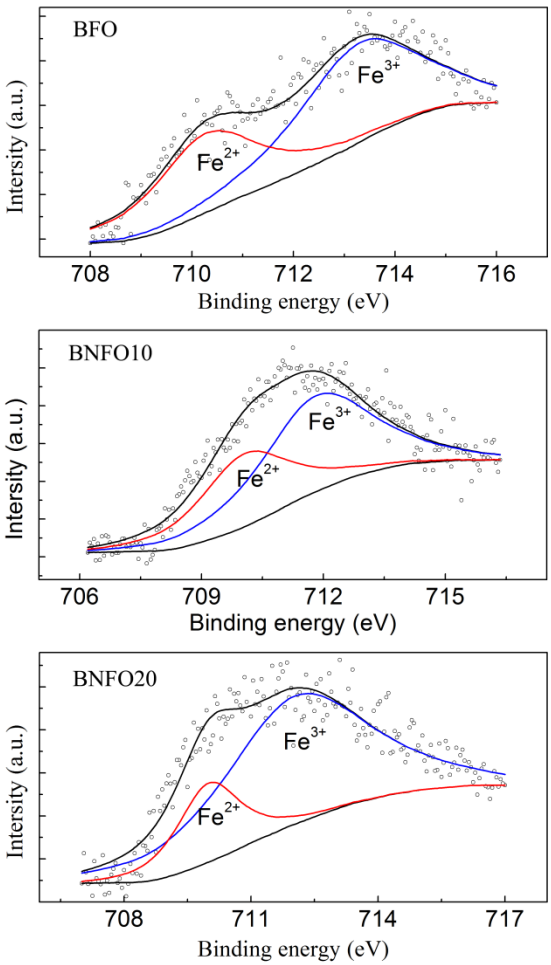

Fig. S6 High-resolution XPS of Fe $2p_{3/2}$ core levels for BFO, BNFO10 and BNFO20. Circle, black line, blue and red lines represent experimental data, fitting data, the peak-fitting simulations of Fe^{3+} and Fe^{2+}, respectively. The appearance of Fe^{2+} reveals oxygen vacancies exist in BFO and BNFO, because Fe^{2+} and oxygen vacancies appear simultaneously for charge compensation in BFO materials.

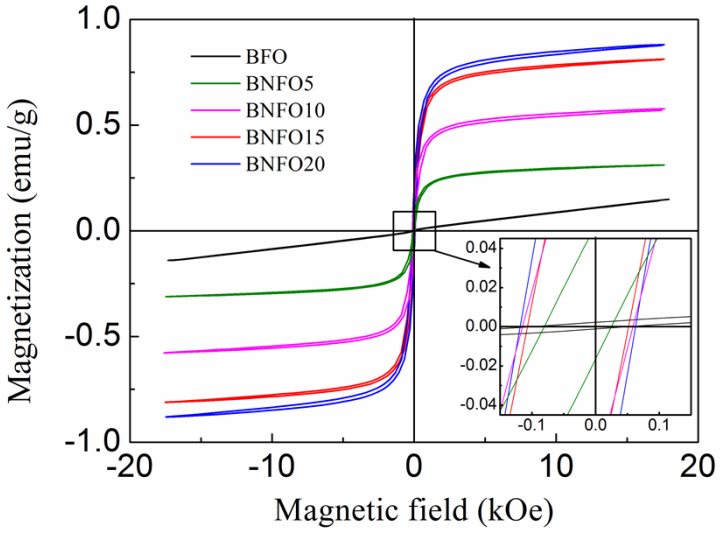

Fig. S7 Hysteresis loops of BFO and BNFO at room temperature.

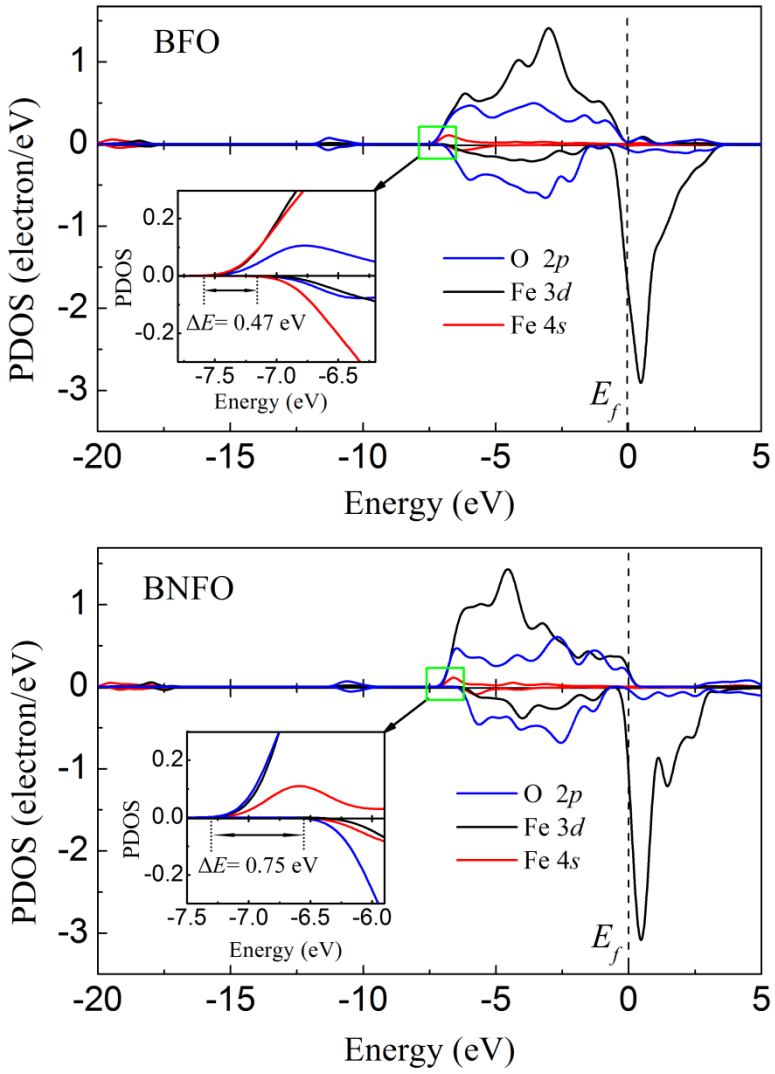

Fig. S8 The densities of states for Fe 3*d*, 4*s* and O 2*p* electrons of BFO and BNFO.

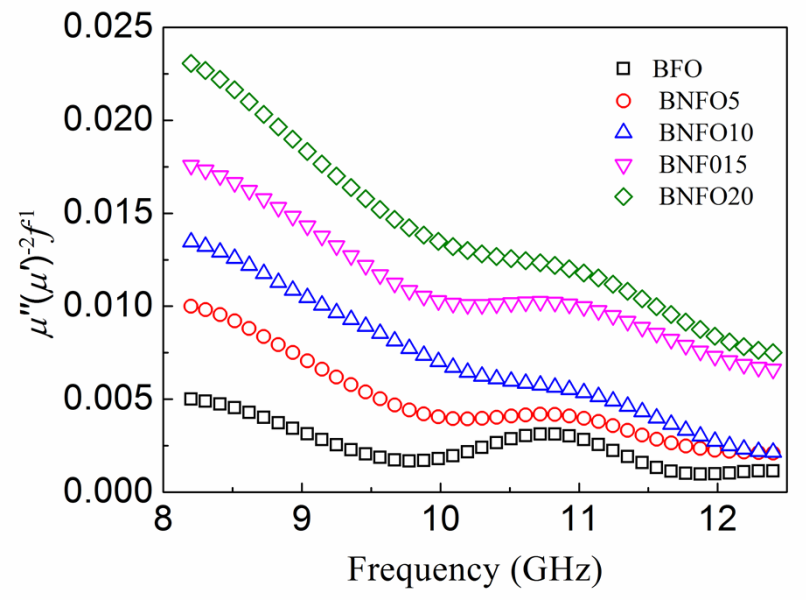

Fig. S9 The eddy current coefficients $\mu''(\mu')^{-2}f^{1}$ of BFO and BNFO versus frequency.

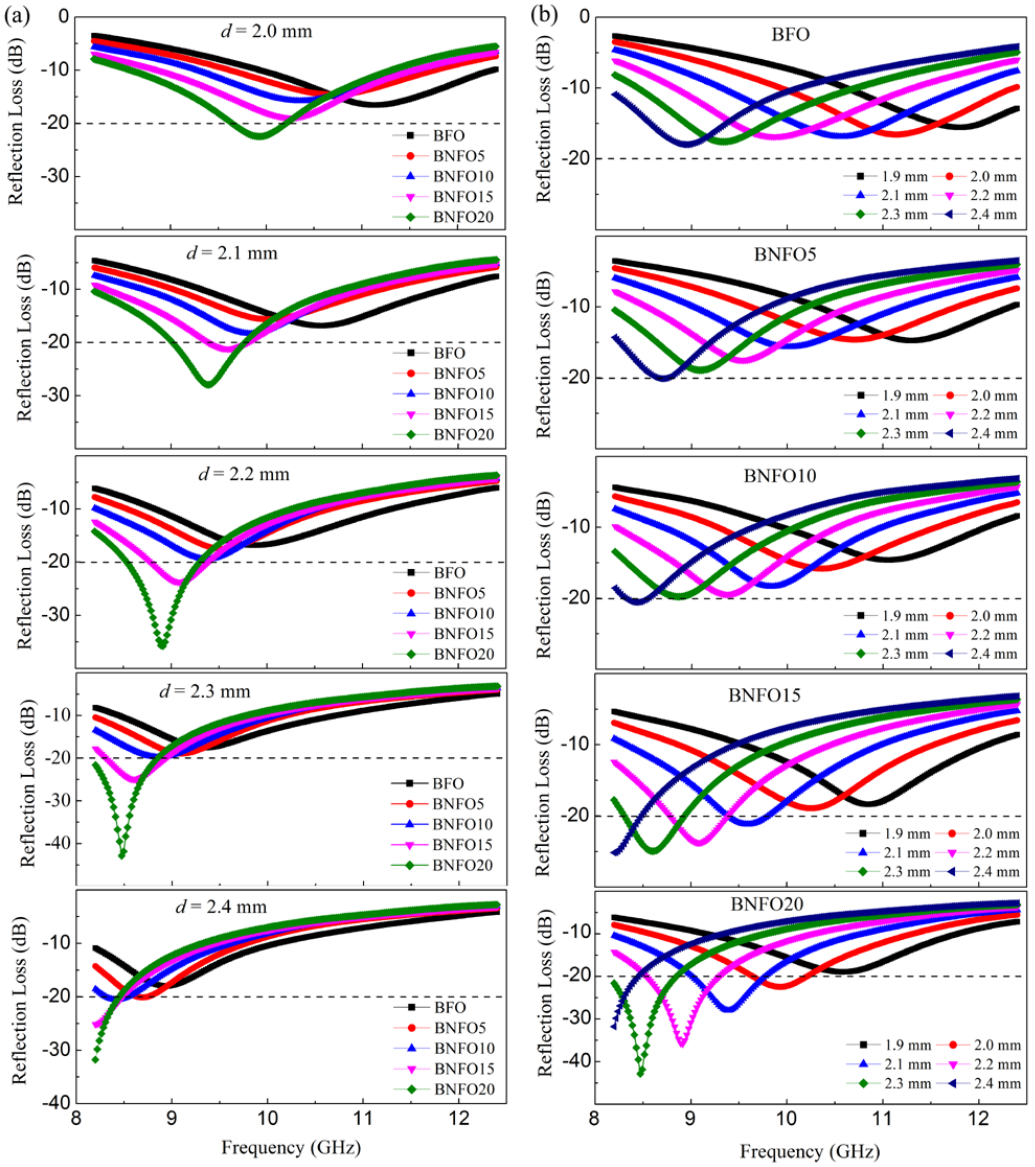

Fig. S10 The *RL* of BFO and BNFO at various (a) Nd concentrations and (b) thicknesses.